J Therm Anal Calorim (2011) 106:355–361
DOI 10.1007/s10973-011-1295-1

Influence of the incorporated metal on template removal from MCM-41 type mesoporous materials

Luiz K. C. de Souza · Juliana J. R. Pardauil · José R. Zamian · Geraldo N. da Rocha Filho · Carlos E. F. da Costa

CBRATEC7 Conference Special Issue

Abstract Al-modified MCM-41, La-modified MCM-41, and Ce-modified MCM-41 mesoporous materials were prepared with different molar ratios (Si/M = 10; 25; 50; 100 and 200) at room temperature. The materials were characterized using XRD, BET–BJH, and TG–DTA. The XRD showed four peaks, due to the ordered hexagonal array of parallel silica tubes, which could be indexed as (100), (110), (200), and (210), assuming a hexagonal unit cell. The surface area decreased as the concentration of the metal incorporated in the material increased. The thermal stability of the materials was around 650 °C. The CeO_2 phase made the mass transfer process more difficult, hindering Hofmann degradation and favoring oxidation.

Keywords Thermal degradation · Surfactant · AlMCM-41 · LaMCM-41 · CeMCM-41

Introduction

Mesoporous materials of the type MCM-41 have attracted considerable attention because of their interesting structure and potential applications in the fields of catalysis and adsorption. As a result of their high surface area, well-defined regular pore shape, and narrow pore-size distribution [1], MCM-41 materials are widely used as catalysts. The MCM-41 structure represents a hexagonal ordering of cylindrical channels consisting of amorphous silica with pore diameters ranging between 15 and 100 Å, depending on the length of the alkyl chains of the surfactant molecules and the synthesis conditions, such as temperature, pH, and time. Much research has been devoted to the incorporation of divalent (Co, Zn), trivalent (Al, Ga, Cr, Fe, Ce, La), and tetravalent (Ti, V, Mn, Sn, Zr) transition and non-transition metal ions in the silica network with the objective to increase catalysis activity because Si-MCM-41 shows low catalysis activity due to its weak acid surface [2]. However, there is no knowledge of the influence of the metal ion or of its interaction with surfactant molecules in the surfactant removal process. Souza et al. [3] evaluated only the variables that determined structure ordering is of fundamental importance in the preparation of mesoporous materials.

In this article, Al-modified MCM-41, La-modified MCM-41, and Ce-modified MCM-41 were prepared at room temperature with different molar ratios (Si/Metal = 10; 25; 50; 100 and 200). The effects of the metal (Al, La, and Ce) and of the Si/Metal molar ratio on the thermal profile of the decomposition of the surfactant molecule were investigated. The materials were characterized by X-ray diffraction (XRD), nitrogen adsorption–desorption (BET–BJH), and thermal analysis (TG–DTA).

Experimental

The synthesis procedure used in this study was carried out at room temperature and based on the work of Cai et al. [4]. A salt of the metal was first dissolved in water under magnetic agitation, to which NH_4OH was added later. Cethyltrimethylammonium bromide (CTAMBr) was separately mixed with water and heated. When the solution became homogenous, it was added to another mixture. Finally, the tetraethylorthosilicate (TEOS) was gradually added to the reaction mixture, with a molar composition of

L. K. C. de Souza · J. J. R. Pardauil · J. R. Zamian · G. N. da Rocha Filho · C. E. F. da Costa (✉)
Laboratório de Catálise e Oleoquímica, ICEN, UFPA, Belém, PA, Brazil
e-mail: emmerson@ufpa.br

1TEOS:XSalt of metal:0.125CTAMBr:69NH_4OH:525 H_2O. After 2 h of agitation, the resulting product was filtered, washed with distilled water, and dried at ambient temperature. During the surfactant removal process, the resulting material was subjected to thermal treatment in a tubular oven at 550 °C for 4 h. The following nomenclature was used: 10MMCM-41, where the number (10, 25, 50, 100, and 200) represented the Si/Metal ratio and M represented the Al, La, or Ce incorporated metal. The materials were characterized by X-ray diffraction (XRD) using a X'pert PRO MPD (PW3040/60) diffractometer from PANalytical (Kα Co) and by N_2 adsorption–desorption at 77 K with a BET–BJH Quantachrome (model Nova 1200). Thermal analyses (TG–DTA) were carried out using a Shimadzu DTG-60H simultaneous analyzer, at a heating rate of 10 °C min^{-1} under dynamic air atmosphere flowing at 50 ml min^{-1}.

Results and discussion

The diffraction patterns of the AlMCM-41 and LaMCM-41 samples synthesized at room temperature are shown in Fig. 1. In Fig. 1, an intense peak is present in the 2θ interval of 2–3°, which can be attributed to the plane reflection at (100). Additionally, three peaks of low intensity are present, which arise from the plane reflections at (110), (200), and (210) and represent the formation of mesoporous materials that are well ordinated with hexagonal symmetry (*p6mm*). After the removal of the surfactant, the behavior of the AlMCM-41 and LaMCM-41 samples with a Si/M ratio of 200 were similar, independent of the type of metal incorporated. The Al and La metals did not cause any major pore arrangement disordering because the (110), (200), and (210) peaks are present, indicating that the two metals are still present in the diffractograms of the respective samples. The diffraction patterns of the 200CeMCM-41 sample are also shown in Fig. 1. Four peaks are seen at (100), (110), (200), and (210), suggesting a high ordination of the hexagonal pore arrangement in the material, in agreement with Araujo et al. [5]. The intense peak from the reflection plane at (100) suggests the formation of the mesopore structure.

For the samples containing a higher quantity of incorporated metal (lower Si/M ratio), greater pore disarrangement is expected due to the increase in the amount of metal incorporated into the MCM/41 structure. Figure 2 shows the diffractograms of the various calcinated samples that have Si/Al and Si/La molar ratios equal to 100, 50, 25, and 10. In Fig. 2, the materials modified with Al had peaks that were more defined than those from the materials modified with La, indicating that a greater pore disarrangement occurred in the materials modified with La. The materials

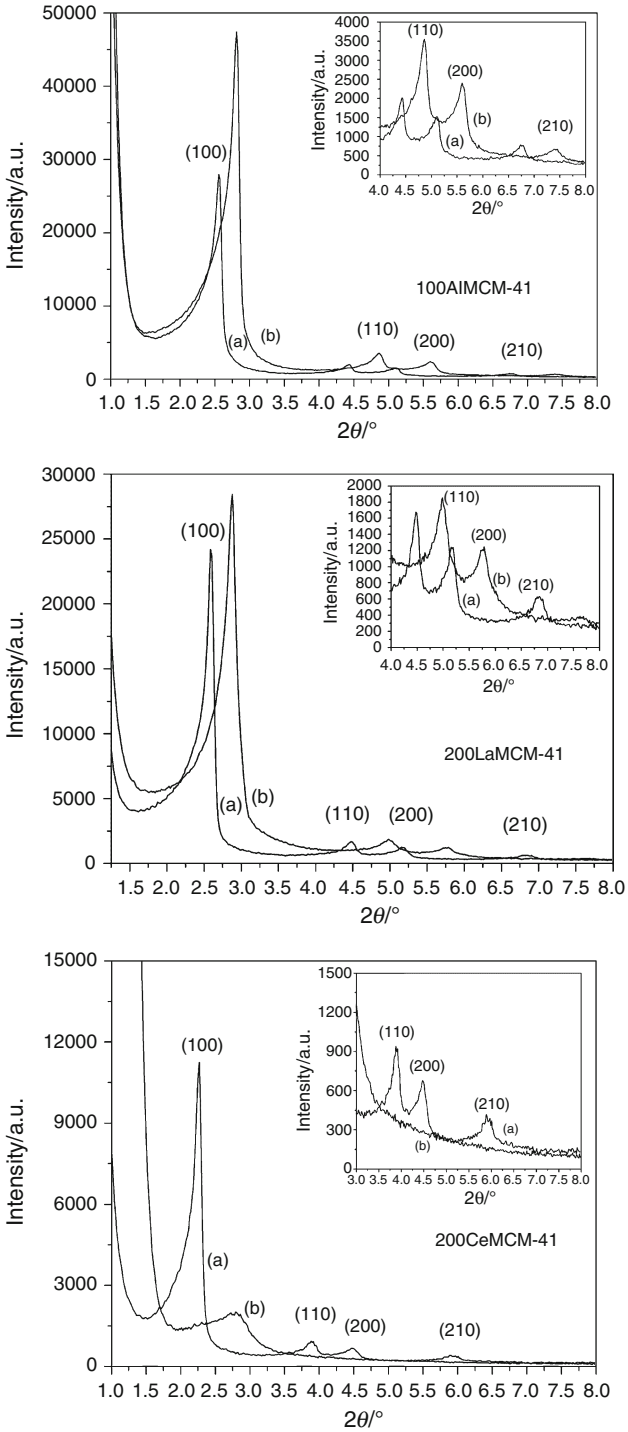

Fig. 1 X-ray diffraction patterns of 100AlMCM-41, 200LaMCM-41, and 200CeMCM-41, **a** as synthesized and **b** calcinated

modified with Ce and had Si/Ce ratios lower than 50 gave only a weak and broad peak at (100), suggesting that a reduction in mesopore ordination occurred as the Ce metal content of the MCM-41 structure increased. This result could be due to a partial substitution of the structural Si^{4+}

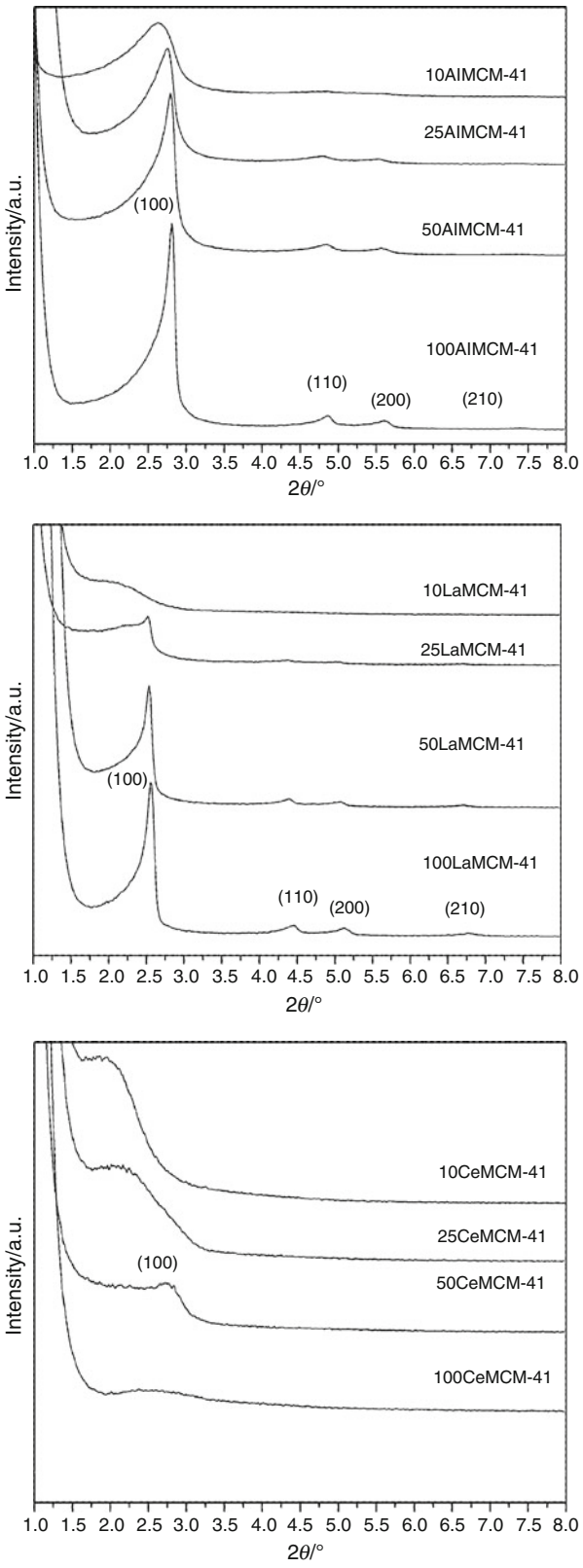

Fig. 2 X-ray diffraction patterns of calcinated samples with Si/Al, Si/La, and Si/Ce ratios equal to 100, 50, 25, and 10

of the MCM-41 for the Ce^{3+} ion, resulting in the disordering of the hexagonal symmetry of the MCM-41.

The diffraction patterns of CeMCM-41 calcinated with Si/Ce molar ratios of 10, 25, 50, 100, and 200 were obtained at a superior angle of 8°. For samples with Si/Ce molar ratios lower than 100, the X-ray diffraction patterns revealed peaks at (111), (200), (220), and (311) corresponding to the cubic structure of the CeO_2 and the spatial group *Fm-3m* (ICSD 2-1306). Because of the larger size of Ce^{3+} compared to Si^4, the formation of this phase can be attributed to the non-incorporation of Ce to the mesopore walls, which thus allows for the formation of CeO_2.

The surface area, pore volume, pore diameter, and pore-size distribution of the materials were determined by investigating their adsorption–desorption of N_2 at 77 K. A high surface area of approximately 1,417 m^2g^{-1} was observed on the MCM-41. Casuscelli et al. [6] found an even higher surface area for the MCM-41 (2,040 m^2/g). As Casuscelli suggested, the incorporation of Ti causes a reduction in the surface area to 1,490 m^2/g for Si/Ti ratios equal to 30. This behavior was confirmed in this study; the surface area indeed decreased as the quantity of incorporated metal increased.

In Table 1, the surface area, pore volume, mean pore diameter, and the wall width for the AlMCM-41 samples are listed. In this table, a reduction in the surface area can be observed as the quantity of incorporated metal in the MCM-41 structure increases. Sun et al. [7] and Ajaikumar et al. [8] studied the incorporation of Al into MCM-41 and determined that increasing the concentration of Al directly led to a reduction in surface area. In Chen et al. [9], the authors found that a reduction in surface area of the AlMCM-41 and LaMCM-41 materials also occurred when the wall width of the mesopores increased.

Other important properties elucidated from the N_2 adsorption–desorption experiments were the pore volume and the pore diameter, which increased proportionally with the concentration of Al due to the incorporation of Al in the sieve structure. This result is not surprising as the Al–O link is longer than the Si–O link. Du et al. [10] examined the incorporation of V in the MCM-41 structure and obtained a similar trend. They found that incorporating V increased the pore diameter of MCM-41 because the transition metal ions are larger in size, thereby resulting in a V–O link that is longer than a Si–O link. Moreover, the sample had a narrow uniform pore-size distribution. Notably, metal incorporation in MCM-41 does not have a regular length because of the amorphous structure that can change the length and angle of the link.

As for the materials modified by Ce, the incorporation of Ce resulted in a reduction in the material's surface area.

Table 1 Physical properties of the mesoporous AlMCM-41materials

Sample	Surface area/mg^2g^{-1}	Pore volume/cm^3g^{-1}	APD[a]/Å	Wall thickness[b]/Å
MCM-41	1,417	0.06	33.96	6.2
200AlMCM-41	1,365	0.09	33.92	7.4
100AlMCM-41	1,155	0.08	33.88	8.5
50AlMCM-41	1,136	0.11	34.16	8.5
25AlMCM-41	1,048	0.10	34.00	8.2
10AlMCM-41	942.6	0.08	34.00	11.0

[a] *APD* average pore diameter (determined using BJH method)

[b] Wall thickness = unit cell parameter (a_0)—APD, where a_0 was obtained from the XRD data using the formula $a_0 = 2d_{100}/3^{1/2}$

Table 2 Mass loss intervals for the mesoporous AlMCM-41materials

Sample	Mass loss/%					
	Temperature range/°C					
	25–110	110–265	265–305	305–395	395–850	Total
MCM-41	6.0	29.5	12.4	3.8	2.9	54.6
200AlMCM-41	6.4	27.3	14.2	4.6	2.9	55.4
100AlMCM-41	5.7	25.2	13.2	5.8	3.4	53.4
50AlMCM-41	6.7	22.7	12.3	6.7	5.1	53.6
25AlMCM-41	7.3	20.4	12.2	7.3	6.2	53.4
10AlMCM-41	7.3	16.8	8.8	10.0	9.3	52.3

One possible explanation for this behavior is that the formation of CeO_2 inside the mesopores causes the mesopores of the MCM-41 structure to be blocked. Anilkumar and Holderich [11] synthesized NbMCM-41 materials to investigate the effect of the formation of Nb_2O_5 on the reduction of the material's surface area and obtained similar results. The interaction of the metal with the superficial hydroxyl group causes the pore walls to contract, reducing the pore size (Morey et al. [12]; Grubert et al. [13]).

The nitrogen isotherms can be classified as Langmuir IV isotherms, according to the IUPAC. MCM-41 materials have a regular pore distribution mainly in the regions where capillary condensation occurs. The isotherms are divided into three regions: region I($P/P_0 < 0.25$) is where monolayers form from the recovering of the pore walls; region II ($0.25 < P/P_0 < 0.45$) is where an increase in adsorbed nitrogen occurs, causing nitrogen capillary condensation inside the uniform mesopores; and region III ($P/P_0 > 4.45$) is associated with adsorption of nitrogen on the external surface of the AlMCM-41, La MCM-41, and CeMCM-41 materials (Fig. 3). An increase in the concentration of the metal can cause a reduction in the amount of adsorbed nitrogen and a lower degree inclination in the same relative pressure, due to a smaller uniformity in pore size. For the CeMCM-41 samples, a new region with $P/P_0 > 0.8$ appeared in the N_2 adsorption–desorption isotherms as the quantity of Ce increased and led to capillary condensation within the interparticle pores (Fig. 3). The pore distributions for the AlMCM-41 and LaMCM-41 materials did not become narrower or change much as a result of the modification. However, the uniformity of the pores of the CeMCM-41 materials was altered significantly upon the introduction of Ce.

The results of the thermal analysis showed that mass loss occurred in four stages. The first stage, as illustrated by an endothermic peak along the DTA curve, occurred at temperatures below 150 °C, with a mass loss of 6% in the MCM-41. This stage was related to the removal of physically adsorbed water (Goworek et al. [14]). Another endothermic peak, signifying the second stage, occurred between 150–250 °C and was caused by the elimination of the trimethylamine ($N(CH_3)_3$) that originated in the decomposition of the surfactant head through Hofmann degradation. During this step (below 250 °C), a major part of the surfactant was removed (29.4% for the MCM-41) by the evaporation of the alkene ($C_{16}H_{32}$), as part of the Hofmann degradation mechanism [15–17]. The elimination of trimethylamine in this stage was confirmed by Keene et al. [18], who detected, with the assistance of a mass spectrometer, hexadecane as the major product (Fig. 4). Goworek et al. [19] also conducted a thermal degradation study of MCM-41 and AlMCM-41 mesoporous materials, using TPD-MS, GC–MS, and NMP to determine the effect of Al on the removal of surfactant molecules. They found

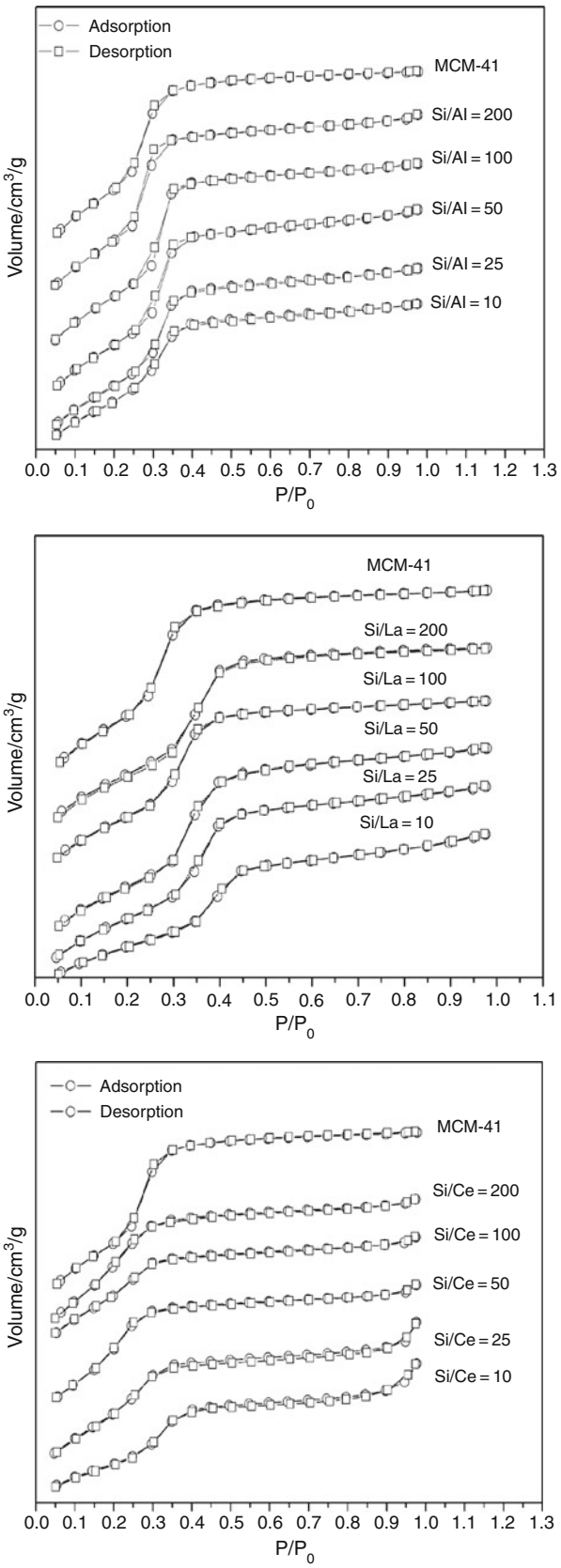

Fig. 3 Nitrogen adsorption/desorption isotherms for the samples AlMCM-41, LaMCM-41, and CeMCM-41

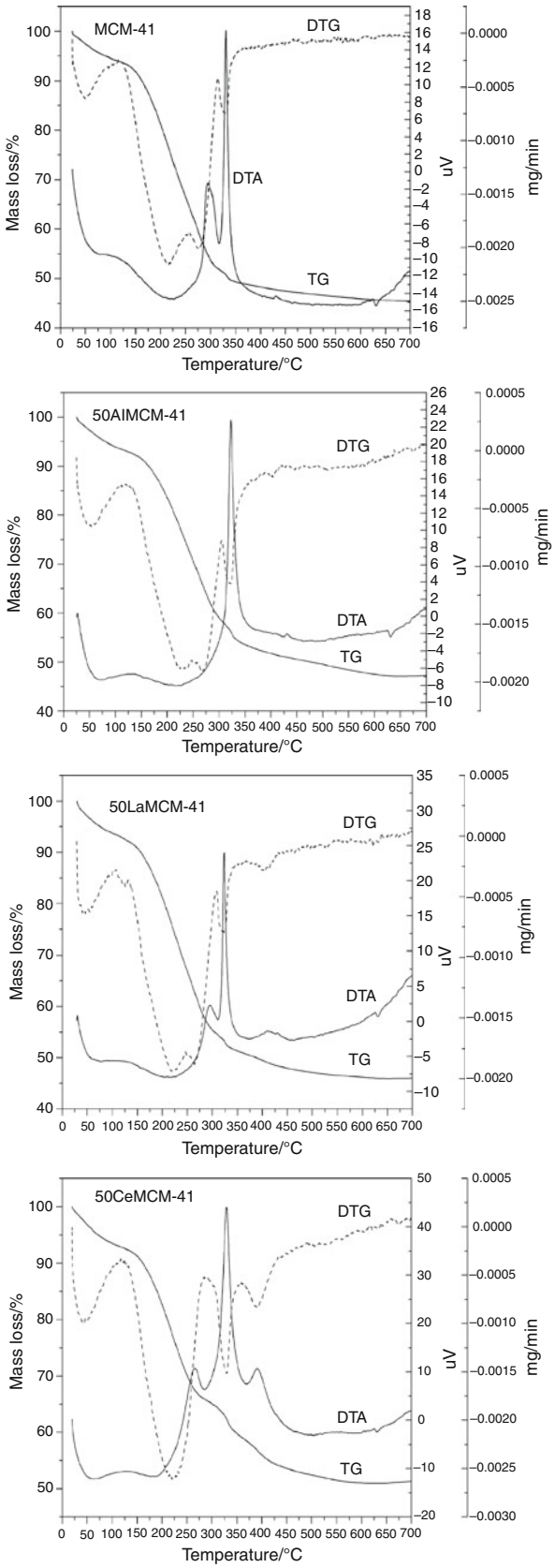

Fig. 4 TG, DTA, and DTG curves for the MCM-41, 50AlMCM-41, 50LaMCM-41, and 50CeMCM-41 samples

Table 3 Mass loss intervals for the mesoporous LaMCM-41 materials

Sample	Mass loss/%						
	Temperature range/°C						
	25–115	115–250	250–314	314–350	350–570	570–850	Total
200LaMCM-41	6.9	25.9	14.7	2.8	2.9	1.0	54.5
100LaMCM-41	6.5	23.1	13.0	2.9	4.6	1.2	51.6
50LaMCM-41	6.5	26.5	12.4	3.8	4.7	2.9	56.9
25LaMCM-41	6.6	23.2	11.3	4.1	5.0	1.0	51.5
10LaMCM-41	7.5	22.2	8.8	3.6	5.7	0.9	48.99

Table 4 Mass loss intervals for the mesoporous CeMCM-41 materials

Sample	Mass loss/%						
	Temperature range/°C						
	25–120	120–300	300–375	375–470	470–600	600–850	Total
200CeMCM-41	7.7	34.4	6.9	4.5	2.9	1.9	58.4
100CeMCM-41	6.8	31.5	6.3	5.8	2.4	0.4	53.4
50CeMCM-41	6.9	27.8	6.1	6.0	2.3	0.4	49.3
25CeMCM-41	5.8	24.7	5.3	8.1	1.6	1.0	46.8
10CeMCM-41	6.3	22.7	4.9	12.3	1.4	0.6	48.3

that the trimethylamine formed at 150 °C in all the samples, agreeing with the results described above, and that at 300 °C, the composite is highly complex and composed of the hexadecene isomers, *N*,*N*-dihexadecylamine and *N*,*N*,*N*-trihexadecylamine.

The third stage of mass loss (12% for MCM-41) was observed on the TG curve, with a corresponding exothermal peak in the DTA curve, in the 250–300 °C temperature range. This stage can be assigned to the premature oxidation of the various fragments of the short carbonic chain, producing CO_2, NO_2, and H_2O. In this step, additional surfactant was removed.

The last stage of mass loss occurred between 300 and 350 °C, when almost all the remaining organic compounds are oxidized to CO_2 and H_2O. However, some trimethylamine can still be present in this stage; Kleitz et al. [16] observed the molecule at 330 °C and suggested that some of the amine groups must interact strongly with the inorganic moieties of the materials, and thus, trimethylamine can be removed completely only at high temperatures. The surfactant wastes may be of the carbonaceous species because a small amount of water was produced by SiOH condensation at temperatures above 350 °C. The amine species and the carbonic chains can rearrange in the mesopores to form a stable polymer, which is easier to oxidize.

The TG–DTG–DTA curves for the AlMCM-41 materials revealed that the temperature at which most of the surfactant was removed increased when the quantity of incorporated Al increased (Table 2). However, in the 305–395 °C temperature range, the mass loss increased more sharply due to an increase in surfactant concentration. This increase caused a higher concentration of the carbonic chains to oxidize at these higher temperatures, and the area of the peak at 395–850 °C in the DTG curve increased. Goworek et al. [19] highlights that the presence of Al in the mesoporous structure leads to a greater isomerization of *n*-hexadecene and to a partial transformation of unsaturated hydrocarbons in other members of the homologous series.

The LaMCM-41 materials exhibited similar thermal behavior (Table 3). However, a new step (350–570 °C) emerged, due to the strong interactions between the surfactant molecules and the surface of the LaMCM-41 materials. The existence of this step suggests that the surfactant molecules interact with varying strengths and are thus removed at different temperature intervals.

In the CeMCM-41 materials, there was a tendency for the amount of organic material removed at the low temperature range (120–300 °C) to decrease when the amount of Ce incorporated in the MCM-41 increased (Table 4). In other words, the relative organic fraction that was submitted to subsequent decomposition and oxidation shifted to higher temperatures.

This trend is most likely due to low yields from the Hofmann degradation process, the consequential favoring of the oxidation process, or by a limitation of mass transfer in this step. Additionally, the formation of the CeO_2 phase, which was described previously and which increased as the

Si/Ce molar ratio decreased, further complicated the process of mass transfer.

Occelli et al. [20] studied the incorporation of Ti and Zr in MCM-41 materials and discovered that the strength of the surfactant–metal interaction forces varied, depending on the metal. The force of interaction increased in the following order: Si-OH < Zr-OH < Ti-OH. In MCM-41, AlMCM-41, LaMCM-41, and CeMCM-41 materials, the surfactant–metal interaction increased in the following order: Si-OH < Al-OH < La-OH < Ce-OH. Additionally, Goworek et al. [19] determined that the chemical specimen interaction with the MCM-41 and AlMCM-41 surface was a determining factor in the removal of the surfactant molecules from the pores of these mesoporous materials and that the nature of the interaction was related to the Bronsted and Lewis acid sites present in MCM-41 and AlMCM-41.

Conclusions

Well-ordered AlMCM-41, LaMCM-41, and CeMCM-41 materials were obtained at room temperature. The surface area decreased from 1,417 m^2/g (MCM-41) to 681 m^2/g (10CeMCM-41) due to an increase in the quantity of incorporated metal in the mesoporous structures. The thermal stability of the materials occurred at approximately 650 °C. The CeO_2 phase made the mass transfer process more difficult and caused the Hofmann degradation to give low yields, thus favoring the oxidation process. Increasing the concentration of incorporated metal reduced the ordering of the mesoporous materials. The interactions between the metals and the surfactant molecules varied in strength, in the following order from weakest to strongest: Si-OH < Al-OH < La-OH < Ce-OH.

Acknowledgements This work was supported by the Graduate Program of Chemistry at Universidade Federal do Pará, Coordenação de Aperfeiçoamento de Pessoal de Nível Superior, and Fundação de Amparo à Pesquisa do Estado do Pará.

References

1. Selvam P, Bhatia SK, Sonwane CG. Recent advances in processing and characterization of periodic mesoporous mcm-41 silicate molecular sieves. Ind Eng Chem Res. 2001;40:3237–61.
2. Zhao Q, Xu Y, Li Y, Jiang T, Li C, Yin H. Effect of the Si/Ce molar ratio on the textural properties of rare earth element cerium incorporated mesoporous molecular sieves obtained room temperature. Appl Surf Sci. 2009;255:9425–9.
3. Souza MJB, Silva AOS, Aquino JMFB, Fernandes VJ Jr, Araújo AS. Kinetic study of template removal of MCM-41 nanostructured material. J Therm Anal Calorim. 2004;75:693–8.
4. Cai Q, Lin W-Y, Xiao F-S, Pang W-Q, Chen X-H, Zou B-S. The preparation of highly ordered MCM-41 with extremely low surfactant concentration. Microporous Mesoporous Mater. 1999;32:1–15.
5. Araujo SA, Araujo AS, Fernandes NS, Fernandes VJ Jr, Ionashiro M. Effect of the catalyst MCM-41 on the kinetic of the thermal decomposition of poly(ethylene terephthalate). J Therm Anal Calorim. 2010;99:465–9.
6. Casuscelli SG, Eimer GA, Canepa A, Heredia AC, Poncio CE, Crivello ME, Perez CF, Aguilar A, Herrero R. Ti-MCM-41 as catalyst for α-pinene oxidation. Study of the effect of Ti content and H_2O_2 addition on activity and selectivity. Catal Today. 2008;133–135:678–83.
7. Sun Y, Yue Y, Gao Z. Synthesis and characterization of AlMCM-41 molecular sieves. Appl Catal A Gen. 1997;161:121–7.
8. Ajaikumar S, Pandurangan A. Esterification of alkyl acids with alkanols over MCM-41 molecular sieves: influence of hydrophobic surface on condensation reaction. J Mol Catal A Chem. 2007;266:1–10.
9. Chen X, Huang L, Ding G, Li Q. Characterization and catalytic performance of mesoporous molecular sieves Al-MCM-41 materials. Catal Lett. 1997;44:123–8.
10. Du G, Lim S, Yang Y, Wang C, Pfefferle L, Haller GL. Catalytic performance of vanadium incorporated MCM-41 catalysts for the partial oxidation of methane to formaldehyde. Appl Catal A Gen. 2006;302:48–61.
11. Anilkumar M, Hölderich WF. Highly active and selective Nb modified MCM-41 catalysts for Beckmann rearrangement of cyclohexanone oxime to epsilon-caprolactam. J Catal. 2008;260:17–29.
12. Morey M, Davidson A, Eckert H, Stucky G. Pseudotetrahedral O3/2V O centers immobilized on the walls of a mesoporous, cubic MCM-48 support: preparation, characterization, and reactivity toward water as investigated by 51 V NMR and UV–Vis spectroscopies. Chem Mater. 1996;8:486–92.
13. Grubert G, Rathouský J, Schulz-ekloff G, Wark M, Zukal A. Reducibility of vanadium oxide species in MCM-41. Microporous Mesoporous Mater. 1998;22:225–36.
14. Goworek J, Borówka A, Zaleski R, Kusak R. Template transformations in preparation of MCM-41 silica. J Therm Anal Calorim. 2005;79:555–60.
15. Cope A, Norman A, Lebe L, Moore PT, Moore WR. Mechanism of the Hofmann elimination reaction: evidence that an ylide intermediate is not involved in simple compounds. J Am Chem Soc. 1961;83:3861–5.
16. Kleitz F, Schmidt W, Schuth F. Evolution of mesoporous materials during the calcination process: structural and chemical behavior. Microporous Mesoporous Mater. 2001;44–45:95–109.
17. Ryczkowski J, Goworek J, Gac W, Pasieczna S, Borowiecki T. Temperature removal of templating agent from MCM-41 silica materials. Thermochim Acta. 2005;434:2–8.
18. Keene MTJ, Gougeon RDM, Denoyel R, Harris RH, Rouquerol J, Llewellyn PL. Calcination of the MCM-41 mesophase: mechanism of surfactant thermal degradation and evolution of the porosity. J Mater Chem. 1999;9:2843.
19. Goworek J, Kierys A, Gac W, Borówka A, Kusak R. Thermal degradation of CTAB in as-synthesized MCM-41. J Therm Anal Calorim. 2009;96:375–82.
20. Occelli ML, Biz S, Auroux A. Effects of isomorphous substitution of Si with Ti and Zr in mesoporous silicates with the MCM-41 structure. Appl Catal A Gen. 1999;183:231–9.